Clinical & Translational Immunology

Australian and New Zealand Society for Immunology Inc.

Clinical & Translational Immunology 2024; e1505. doi: 10.1002/cti2.1505
www.wileyonlinelibrary.com/journal/cti

ORIGINAL ARTICLE

Chitinase 3-like 1 expression associated with lymphatic metastasis and prognosis in urothelial carcinoma of the bladder

Bo Wang[1,2,a], Ke Chen[1,a], Mingchao Gao[1,a], Xi Sun[1], Wang He[1], Junyu Chen[1], Wenjuan Yang[3], Tenghao Yang[1], Haide Qin[2], Honglian Ruan[4], Hao Huang[1], Tianxin Lin[1,2] & Jian Huang[1]

[1]Department of Urology, Sun Yat-sen Memorial Hospital, Sun Yat-sen (Zhongshan) University, Guangzhou, China
[2]Guangdong Provincial Key Laboratory of Malignant Tumor Epigenetics and Gene Regulation, Guangdong-Hong Kong Joint Laboratory for RNA Medicine, Medical Research Center, Sun Yat-Sen Memorial Hospital, Sun Yat-sen (Zhongshan) University, Guangzhou, China
[3]Department of Hematology, Sun Yat-sen Memorial Hospital, Sun Yat-sen (Zhongshan) University, Guangzhou, China
[4]School of Public Health, Guangzhou Medical University, Guangzhou, China

Correspondence
H Huang, T Lin and J Huang, Department of Urology, Sun Yat-sen Memorial Hospital, Sun Yat-sen (Zhongshan) University, Guangzhou 510120, China.
E-mails:
huangh269@mail.sysu.edu.cn;
lintx@mail.sysu.edu.cn and
huangj8@mail.sysu.edu.cn

[a]Equal contributors.

Received 13 November 2023;
Revised 4 March 2024;
Accepted 26 March 2024

doi: 10.1002/cti2.1505

Clinical & Translational Immunology
2024; **13**: e1505

Abstract

Objectives. Lymphatic metastasis, an early stage of the metastasis process, is associated with adverse clinical outcomes in urothelial carcinoma of the bladder (UCB). However, the role of inflammation in triggering lymphatic metastasis remains unclear. **Methods.** We employed an RNA-sequencing cohort ($n = 50$) from Sun Yat-Sen Memorial Hospital (SYMH) to identify the most highly upregulated inflammatory gene associated with lymphatic metastasis. Using immunohistochemistry and immunofluorescence analyses, we validated the association of the identified molecule with clinical features and prognosis in an independent UCB cohort ($n = 244$) from SYMH. We also analysed TCGA-BLCA cohort ($n = 408$) to identify its potential biological pathways and immune landscape. **Results.** In our study, chitinase 3-like 1 (CHI3L1) emerged as a significantly overexpressed proinflammatory mediator in UCB tissues with lymphatic metastasis compared to those without lymphatic metastasis (81.1% vs. 47.8%, $P < 0.001$). Within UCB tissues, CHI3L1 was expressed in both stromal cells (52.8%) and tumor cells (7.3%). Moreover, CHI3L1$^+$ stromal cells, but not tumor cells, exhibited independent prognostic significance for both overall survival ($P < 0.001$) and recurrence-free survival ($P = 0.006$). CHI3L1$^+$ stromal cells were positively associated with D2-40$^+$ lymphatic vessel density ($P < 0.001$) and the immunosuppressive PD-L1/PD-1/CD8 axis in UCB tissues (all $P < 0.05$). A bioinformatics analysis also identified a positive association between CHI3L1 expression and lymphangiogenesis or immunosuppression pathways. **Conclusion.** Our study established a clear association between stromal CHI3L1 expression and

lymphatic metastasis, suggesting that stromal CHI3L1 expression is a potential prognostic marker for bladder cancer patients.

Keywords: biomarkers, CHI3L1, lymphatic metastasis, urothelial carcinoma of the bladder

INTRODUCTION

Bladder cancer ranks among the most prevalent urological malignancies, with urothelial carcinoma of the bladder (UCB) being the predominant form in the majority of cases.[1] Patients with lymph node (LN) metastasis experience significantly reduced 5-year survival rates compared to those without it (25–31% vs. 49–57%).[2,3] LN metastasis is a multifaceted process involving intricate communication between tumor cells and various stromal cells through the release of lymphangiogenic growth factors (such as vascular endothelial growth factor C [VEGF-C]) or the induction of immune suppression (e.g. programmed cell death protein 1/programmed death ligand 1 [PD-1/PD-L1] axis).[4–6] Previous studies primarily focused on the role of tumor cells in lymphatic metastasis.[2,4,7] The identification of stromal mediators responsible for instigating lymphatic metastasis is of great significance since they may emerge as novel prognostic markers within clinical tumor pathologies, offering new avenues for future therapeutic interventions.

The chitinase 3-like 1 (CHI3L1, also known as YKL-40) gene is a member of the evolutionarily conserved 18-glycosyl hydrolase (*GH 18*) gene family in mammals.[8] It plays crucial roles in maintaining biological homeostasis, including functions in pathogen defence, inflammation, tissue repair and remodelling.[8–10] In the context of cancer, CHI3L1 can be induced by both tumor cells and various stromal cells, including macrophages, neutrophils, fibroblast-like cells, endothelial cells and embryonic stem cells.[10,11] CHI3L1 is involved in diverse aspects of tumor progression.[10,12] First, it directly influences tumor cells by promoting cell proliferation, invasion and metastasis.[13] Second, it acts as an angiogenic factor that stimulates tumor angiogenesis either independently or in a VEGF-dependent pathway.[14,15] Third, in mouse models, CHI3L1 enhances tumor progression and lymphatic spread by creating an immunosuppressive tumor microenvironment (TME).[16] In humans, a substantial body of evidence has demonstrated an inverse association between increased serum CHI3L1 levels and disease-free survival in various cancers, including colorectal cancer, glioblastoma, breast cancer, ovarian carcinoma and gastric cancer.[11,17–19] However, the clinical significance of CHI3L1 expression and its underlying functional mechanisms in bladder cancer tissues remain unclear.

This study aims to investigate the significance of CHI3L1 expression in UCB tissues and assess its relationship with lymphatic metastasis within the TME. We conducted a transcriptomic analysis to pinpoint CHI3L1 as a potential biomarker associated with lymphatic metastasis in UCB patients. An immunohistochemical (IHC) analysis was carried out to gauge the expression of CHI3L1 in tumor tissues and correlate this expression with clinical outcomes in a cohort of 244 UCB patients. In addition, we conducted multiplex immunofluorescence (MIF) and IHC analyses to examine the connection among CHI3L1 expression, D2-40$^+$ lymphatic vessel density (LVD), CD105$^+$ micro-vessel density (MVD) as well as immunosuppressive components, including the PD-L1/PD-1/CD8 axis and other immune checkpoint molecules. Bioinformatic analysis was employed to identify potential biological pathways and immune landscape of CHI3L1 in UCB patients.

RESULTS

CHI3L1 was identified as an important lymphatic metastasis-related gene

We utilised bulk RNA-sequencing (RNA-seq) data from UCB cohort I of Sun Yat-Sen Memorial Hospital (SYMH, $n = 50$, Supplementary table 1) to pinpoint stromal mediators associated with lymphatic metastasis. Differentially expressed genes (DEGs) related to tumors, defined as tumor-related genes (TRGs), were discovered between the tumor and peri-tumor groups (Figure 1a). Similarly, DEGs related to lymphatic metastasis, defined as lymphatic metastasis-related genes (LRGs), were identified between the LN$^+$ and LN$^-$ groups (Figure 1b). We identified 30 unique genes that resided at the intersection of LRGs and TRGs (Figure 1c). Among them, *CHI3L1* emerged as the most prominently upregulated lymphatic

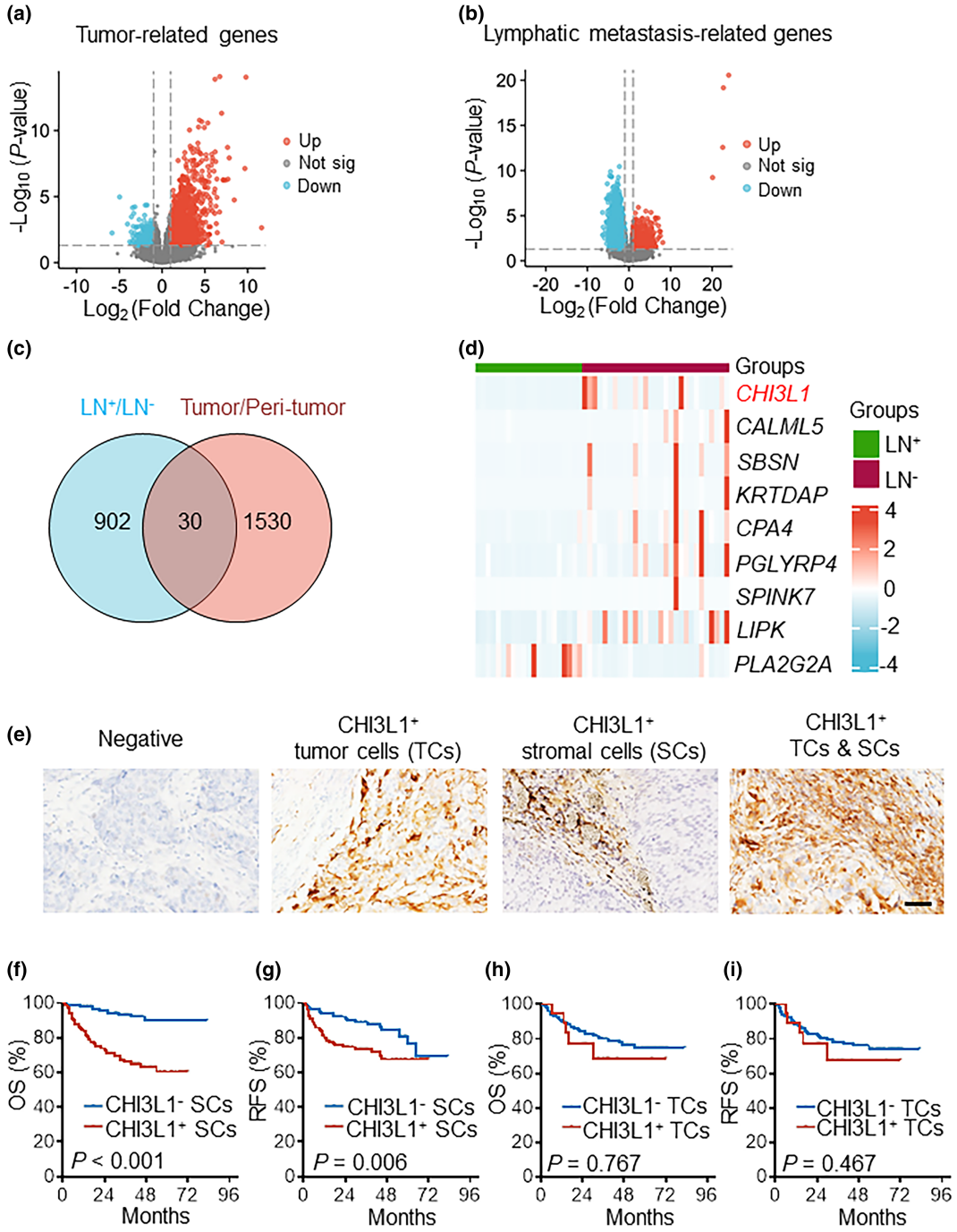

Figure 1. CHI3L1 is predominantly expressed in stromal cells within urothelial carcinoma of the bladder (UCB) tissues. **(a)** Differentially expressed genes between UCB primary tumor tissues (n = 50) and some of the matched peritumor tissues (n = 8). **(b)** Differentially expressed genes between UCB primary tumor tissues with lymph node (LN) metastasis (LN^+, n = 29) and without LN metastasis (LN^-, n = 21). **(c)** The Venn diagram illustrated the intersection of 30 genes between lymphatic metastasis-related genes and tumor-related genes. **(d)** The heatmap displayed *CHI3L1* emerged as the most prominently upregulated inflammatory-associated gene within these 30 genes. **(e)** Representative immunohistochemistry staining images of CHI3L1 (brown) in tumor cells (TCs), stromal cells (SCs) or both TCs and SCs. Scale bar, 50 μm. **(f–i)** Kaplan–Meier curves for overall survival (OS) and recurrence-free survival (RFS) in UCB patients stratified by **(f, g)** $CHI3L1^+$ SCs and **(h, i)** $CHI3L1^+$ TCs. *P*-values were calculated using the log-rank test. Statistical significance is indicated by *P*-values.

Table 1. Association of CHI3L1 expression in tumor cells and stromal cells with the clinical features of UCB patients (n = 244)

	CHI3L1$^+$ tumor cells				CHI3L1$^+$ stromal cells			
Variable	Negative	Positive	*R*	*P*	Negative	Positive	*R*	*P*
No. of patients	226	18			115	129		
Age, years								
≤ 60	101	7	0.031	0.818	58	50	0.117	0.088
> 60	125	11			57	79		
Gender								
Male	193	15	0.015	0.735	100	108	0.046	0.596
Female	33	3			15	21		
Tumor size, cm								
≤ 3	81	9	−0.077	0.345	53	37	0.180	**0.007**
>3	145	9			62	92		
Multifocality								
Unifocal	129	14	−0.110	0.142	60	83	−0.123	0.072
Multifocal	97	4			55	46		
TNM stage								
0/0is/I–II	168	13	0.013	0.786	98	83	0.238	< **0.001**
III–IV	58	5			17	46		
Histological grade								
Low	51	1	0.109	0.133	40	12	0.311	< **0.001**
High	175	17			75	117		
Extent of operation								
TURBT	86	5	0.056	0.539	55	36	0.206	**0.002**
Radical cystectomy	140	13			60	93		

CHI3L1, chitinase 3-like 1; TURBT, transurethral resection of bladder tumor; UCB, urothelial carcinoma of the bladder.
Differences between groups were calculated using the Wilcoxon signed-rank test. Significant *P*-values are shown in bold.

metastasis-related inflammatory gene in UCB tissues (log_2 fold change = 3.35, Figure 1d).

CHI3L1 was mainly expressed in stromal cells in UCB tissues

We conducted IHC staining to assess the protein level of CHI3L1 in an independent UCB cohort II of SYMH (n = 244). The expression of CHI3L1 was discerned as being broadly distributed, with variable cytoplasmic staining observed in tumor cells and/or stromal cells (Figure 1e). Among the complete set of specimens, approximately 7.3% (18 of 244) exhibited CHI3L1$^+$ tumor cells, while a more substantial 52.8% (129 of 244) displayed CHI3L1$^+$ stromal cells. Notably, 11 patients, accounting for 4.5% of the total (11 of 244), presented CHI3L1-positive expression in both tumor cells and stromal cells.

CHI3L1$^+$ stromal cells were associated with clinical features and diminished survival

To investigate the relationship among CHI3L1 expression, clinical characteristics and patient survival, a comprehensive analysis was carried out within the UCB cohort II (n = 244, Table 1). The findings revealed a positive correlation between CHI3L1$^+$ stromal cells and aggressive clinical features, including tumor size (P = 0.007), TNM stage (P < 0.001), histological grade (P < 0.001) and extent of surgery (P = 0.002). In contrast, CHI3L1$^+$ tumor cells exhibited no significant association with these clinical parameters.

Regarding survival analysis, CHI3L1$^+$ stromal cells were significantly associated with reduced overall survival (OS, P < 0.001, Figure 1f) and recurrence-free survival (RFS, P = 0.006, Figure 1g). Conversely, CHI3L1$^+$ tumor cells did not exhibit an association with OS (P = 0.767, Figure 1h) or RFS (P = 0.467, Figure 1i). In the univariate analysis, CHI3L1$^+$ stromal cells – along with age, tumor size, multifocality, TNM stage, histological grade and extent of surgery – were identified as prognostic variables for both OS and RFS in UCB patients (Table 2). The significant prognostic variables from the univariate analysis (P < 0.1) were subsequently incorporated into the multivariate analysis, where CHI3L1$^+$ stromal cells retained their status as an independent prognostic factor for poorer OS and RFS, along with TNM stage (Table 2).

Table 2. Univariate and multivariate analyses of factors associated with mortality and recurrence in UCB patients (n = 244)

	Mortality				Recurrence			
		Multivariate				Multivariate		
Variable	Univariate	HR	95% CI	*P*-value	Univariate	HR	95% CI	*P*-value
Age, years (> 60 vs. ≤ 60)	**0.025**	1.786	0.988–3.228	0.055	**0.029**	1.749	0.968–3.159	0.064
Gender (female vs. male)	0.553			NA	0.578			NA
Tumor size (> 3 vs. ≤ 3 cm)	**0.009**	1.456	0.723–2.930	0.293	**0.013**	1.467	0.723–2.975	0.288
Multifocality (multifocal vs. unifocal)	**0.035**	0.701	0.384–1.280	0.247	**0.041**	0.730	0.400–1.333	0.305
TNM stage (III–IV vs. 0/0is/I–II)	< **0.001**	5.905	2.775–12.566	< **0.001**	< **0.001**	5.545	2.647–11.615	< **0.001**
Histological grade (high vs. low)	**0.022**	0.650	0.235–1.800	0.407	**0.021**	0.701	0.252–1.951	0.496
Extent of operation (RC vs. TURBT)	**0.013**	0.692	0.314–1.524	0.360	**0.040**	0.596	0.274–1.297	0.192
CHI3L1$^+$ tumor cells (positive vs. negative)	0.379			NA	0.452			NA
CHI3L1$^+$ stromal cells (positive vs. negative)	< **0.001**	3.607	1.686–7.716	< **0.001**	< **0.001**	3.788	1.766–8.123	< **0.001**

CHI3L1, chitinase 3-like 1; CI, confidence interval; HR, hazard ratio; NA, not applicable; RC, radical cystectomy; TURBT, transurethral resection of bladder tumor; UCB, urothelial carcinoma of the bladder.
Variables associated with mortality or recurrence in the univariate analysis were adopted as covariates in the multivariate Cox regression analysis. Significant *P*-values are shown in bold. HR > 1 = increased risk; HR < 1 = decreased risk.

Furthermore, a subgroup analysis was performed in UCB cohort II, stratified by tumor stage. It indicated that CHI3L1$^+$ stromal cells were predictive of worse OS and RFS in patients with both muscle-invasive bladder cancer (n = 125, P = 0.002 and 0.001, Supplementary figure 1a, b) and non-muscle-invasive bladder cancer (n = 119, P = 0.026 and 0.002, Supplementary figure 1c, d). Similarly, when stratified by histological grade, CHI3L1$^+$ stromal cells significantly predicted reduced OS and RFS in UCB patients with high histological grade (n = 192, all P < 0.001, Supplementary figure 1e, f). However, no correlation was observed between CHI3L1$^+$ stromal cells and OS or RFS in UCB patients with low histological grade (n = 52, all P > 0.05, Supplementary figure 1 g, h).

Nomogram based on CHI3L1$^+$ stromal cells and TNM stage for OS

After observing that CHI3L1$^+$ stromal cells and TNM stage proved to be independent prognostic indicators for OS in the multivariate analysis, we developed a nomogram in UCB cohort II that combined CHI3L1$^+$ stromal cells and TNM stage to predict 3- and 5-year OS (Figure 2a). The calibration curve demonstrated strong concordance between the nomogram-predicted 3- and 5-year OS and the observed 3- and 5-year OS (C-index, 0.802; 95% CI, 0.777–0.828; Figure 2b and c). The decision curve analysis revealed a favorable positive net benefit when predicting 3- and 5-year OS (Figure 2d and e). Notably, the prognostic accuracy of the nomogram model for predicting 3-year OS (area under the curve [AUC] 0.846) or 5-year OS (AUC 0.789) surpassed that of the TNM stage alone (AUC 0.798 for 3-year OS and AUC 0.728 for 5-year OS, respectively, Figure 2f and g).

Association of CHI3L1$^+$ stromal cells with lymphangiogenesis

The lymphangiogenesis pathway plays a pivotal role in facilitating the lymphatic metastasis of tumor cells.[20] In the cancer genome atlas urothelial bladder carcinoma (TCGA-BLCA) cohort, the gene set enrichment analysis (GSEA) analysis demonstrated significant enrichment of the 'LYMPH_ANGIOGENESIS_PATHWAY' in the high *CHI3L1* expression group (P = 0.014, Figure 3a), suggesting that CHI3L1 may play a role in lymphangiogenesis in UCB patients. Additionally, the IHC analysis revealed that CHI3L1$^+$ stromal cells demonstrated a positive association with LN status in UCB patients (n = 244, P < 0.001; Supplementary figure 2a, b). We then generated a heatmap depicting the expression of lymphangiogenesis-related genes concerning *CHI3L1* expression (Figure 3b). Notably, *CHI3L1* expression exhibited a positive association with *VEGFC* and platelet-derived growth factor subunit B (*PDGFB*), but a negative association with vascular endothelial growth factor A (*VEGFA*). In the RNA-seq data from the UCB cohort I (n = 50), *VEGFC*, *PDGFB* and *VEGFA* were all highly expressed in patients with LN$^+$ metastasis status (all P < 0.05, Supplementary figure 2c–e). Moreover, a positive correlation was observed between expression levels

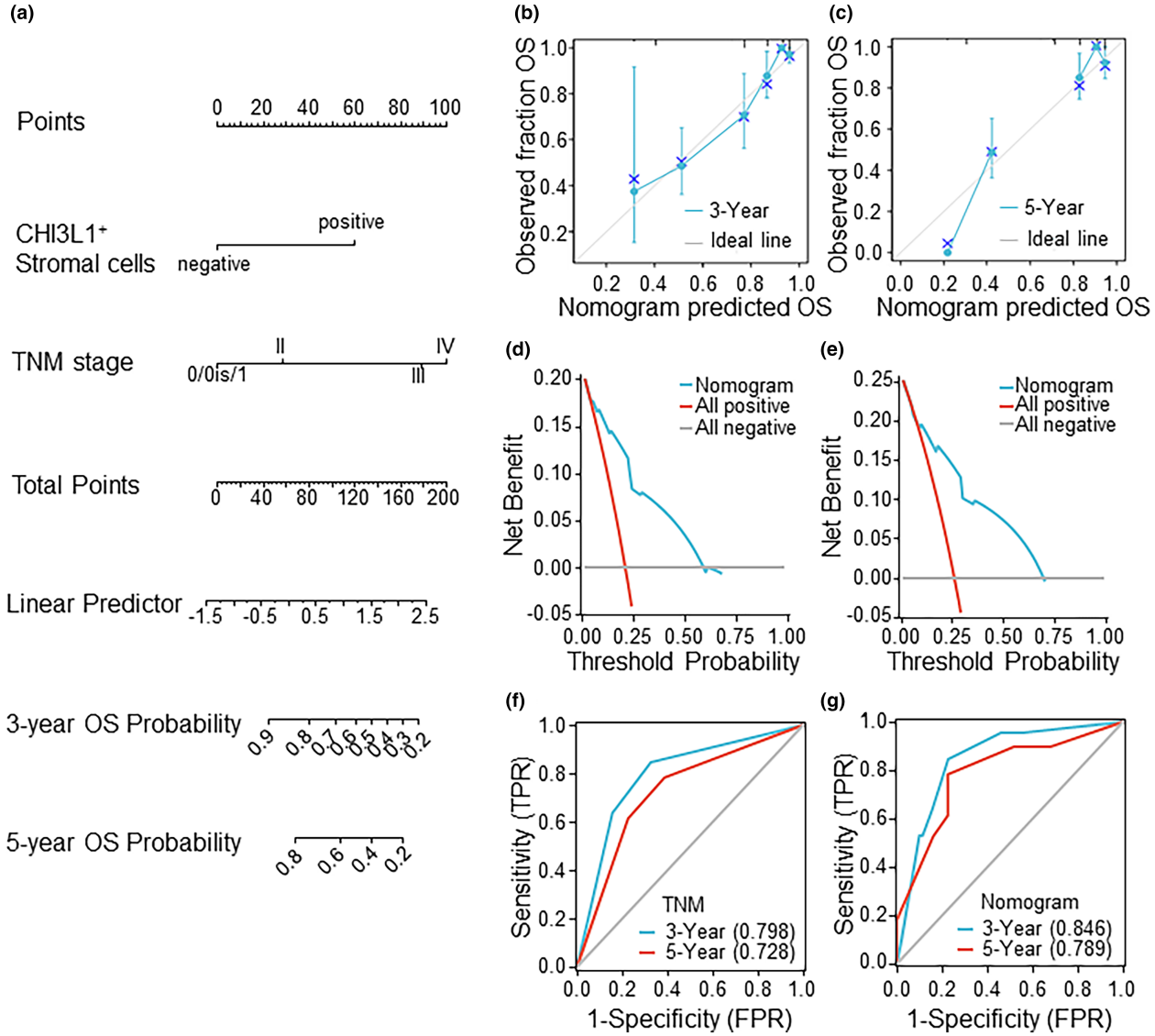

Figure 2. Nomogram for combining CHI3L1$^+$ stromal cells and TNM stage to predict overall survival (OS). **(a)** The nomogram model integrates CHI3L1$^+$ stromal cells and TNM stage to predict 3- and 5-year OS rates. Patients receive scores based on their CHI3L1$^+$ stromal cells and TNM stage (0–IV), and the total points are calculated by summing these scores. **(b, c)** Calibration plots show the predictive performance of the nomogram for OS at 3 and 5 years in urothelial carcinoma of the bladder patients (n = 244). **(d, e)** Decision curve analysis for OS at 3 and 5 years. **(f, g)** Receiver–operating characteristic analysis of the OS based on nomogram and TNM stage at 3 and 5 years. The area under the curve showed the probability of OS at 3 and 5 years respectively.

of *CHI3L1* and *VEGFC* (R = 0.461, P < 0.0001) or *PDGFB* (R = 0.491, P < 0.0001), while a negative correlation was observed between expression levels of *CHI3L1* and *VEGFA* in this cohort (R = −0.477, P < 0.0001, Supplementary figure 2f–h). To further validate these findings, we assessed mRNA expression levels of *CHI3L1*, *VEGFC*, *PDGFB* and *VEGFA* in UCB patients through real-time reverse-transcription PCR (qRT-PCR, n = 12, Figure 3c). The results indicated that *CHI3L1*, *VEGFC* and *PDGFB* expression were significantly higher in tissues from patients with LN metastasis than in those from patients without LN metastasis, while *VEGFA* expression was significantly lower in patients with LN metastasis when than in those without LN metastasis (Figure 3c).

MIF staining analysis further indicated a widespread presence of D2-40$^+$ lymphatic

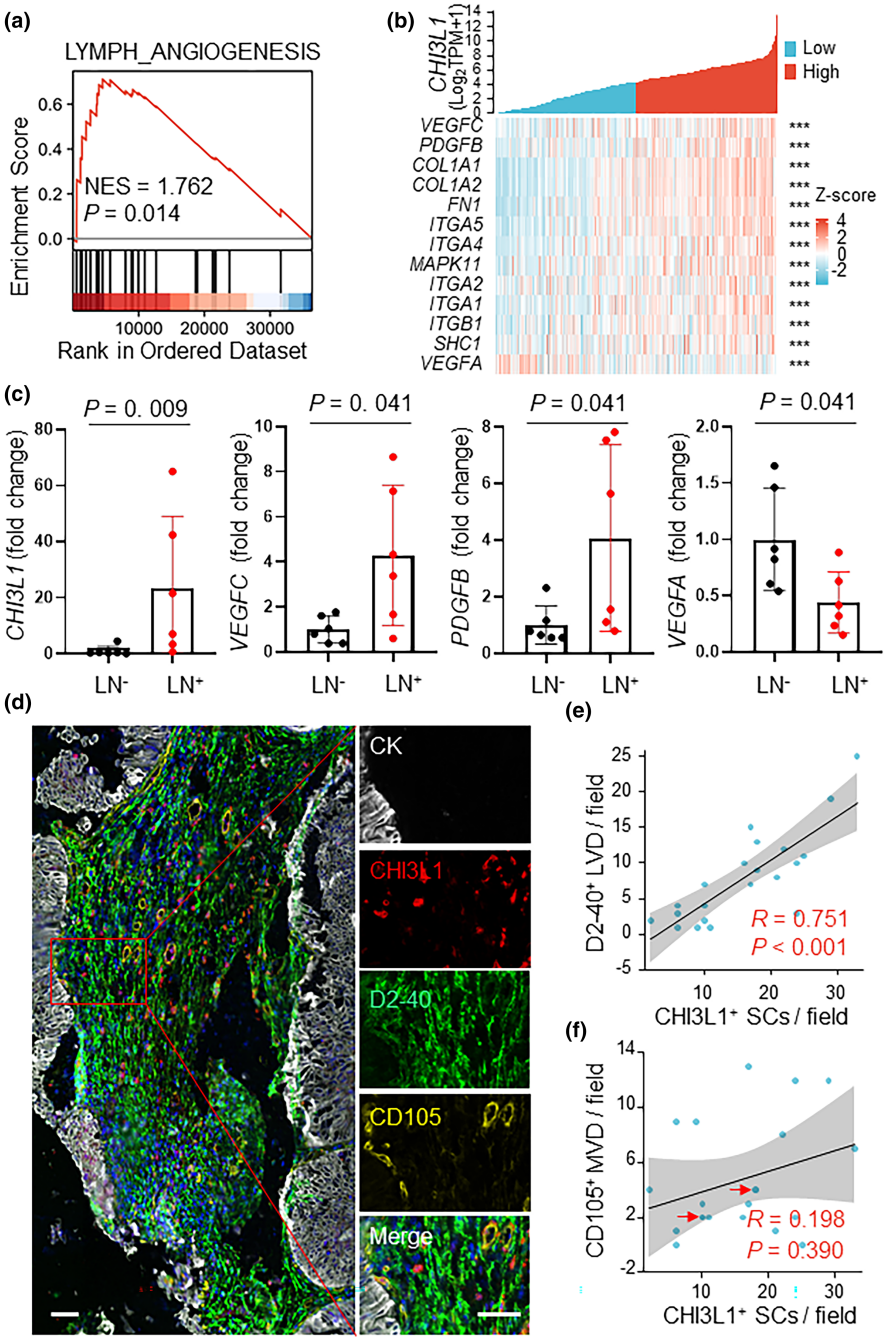

Figure 3. Positive association of CHI3L1 expression with lymphangiogenesis. **(a)** Enrichment plots from gene set enrichment analysis results reveal the 'Lymph_Angiogenesis' pathway enriched in urothelial carcinoma of the bladder (UCB) patients with high *CHI3L1* expression in the TCGA-BLCA cohort. **(b)** Heatmap displaying the core enrichment genes of the lymphangiogenesis pathway and their expression to *CHI3L1* in the TCGA-BLCA cohort. **(c)** Results of qRT-PCR assay illustrating the mRNA expression of *CHI3L1*, *VEGFC*, *PDGFB* and *VEGFA* in our patients (n = 12). **(d)** Representative images of four-colour immunofluorescence staining, showing CHI3L1 (red), the lymphatic endothelium marker (D2-40, green), the vascular endothelium marker (CD105, yellow) and the cytokeratin marker (CK, white), with counterstaining using 4′,6-diamidino-2-phenylindole (DAPI, blue). Scale bars, 50 μm. **(e, f)** Scatter plots indicate the associations of $CHI3L1^+$ stromal cells with lymphatic vessel density (LVD) **(e)** or micro-vessel density (MVD) **(f)** in UCB tissues. In the correlation analysis between $CHI3L1^+$ stromal cells and MVD, there are two cases of overlapped data, marked with red arrows. A significance level of $P < 0.05$ was considered statistically significant. Statistical significance was determined by the unpaired *t*-test and is indicated by *P*-values. ***$P < 0.001$.

endothelial cells in stromal regions with intense CHI3L1$^+$ stromal cells (Figure 3d). CHI3L1$^+$ stromal cells were positively correlated with D2-40$^+$ LVD, but not with CD105$^+$ MVD within the stromal area of tumor tissues (n = 21 fields, Figure 3e and f). These results suggested a positive association of CHI3L1 expression with lymphangiogenesis in UCB tissues.

Clinical value of CHI3L1$^+$ stromal cells with immunosuppressive TME in UCB patients

Previous studies have observed the immunosuppressive TME, including the PD-L1/PD-1/CD8 pathway, to be associated with tumor lymphatic metastasis.[21] In the TCGA-BLCA cohort, the GSEA analysis revealed a significant enrichment of the 'Exhausted CD8$^+$ T-cells' pathway in the high *CHI3L1* expression group (P = 0.004, Figure 4a). Single-sample GSEA indicated a positive correlation between *CHI3L1* expression and CD8$^+$ T cells in UCB samples (Figure 4b). Further analysis revealed the high *CHI3L1* expression group displayed significantly elevated levels of genes associated with immunosuppression, including *CD274, PDCD-1*, *TIGIT*, *VSIR*, *HAVCR2* and *LAG3* (Figure 4c). We further explored the *CHI3L1* expression pattern in published data of eight UCB tissues via single-cell RNA-seq (scRNA-seq) analysis.[22] We identified 16 major cell types according to expression of canonical gene markers, including regulatory T cells (Tregs), fibroblasts, plasma cells, basal cells, cytotoxic CD8$^+$ T cells, mast cells, maternal endothelial cells, endothelial cells, MARCO$^-$ macrophages, muscle cells, suprabasal epithelial cells, myeloid cells, lymphatic endothelial cells, CD4$^+$ T cells, B cells and activated dendritic cells (DC, Supplementary figure 3a). The *CHI3L1* expression was enriched in stromal cell populations, including fibroblasts, muscle cells, MARCO$^-$ macrophages and Tregs (Supplementary figure 3b). Among them, fibroblasts were the main product of *CHI3L1* in these eight UCB patients. To further analyse the relationship between *CHI3L1* expression and immunosuppressive TME on a single-cell level, the eight UCB patients were divided into a high group (n = 3) and a low group (n = 5) according to the central tendency of the distribution of *CHI3L1* gene expression within fibroblasts (Supplementary figure 3c). Correlation analysis showed that high *CHI3L1* expression was positively associated with high ratios of *CD274* and *HAVCR2* expression on activated DCs; high ratios of *HAVCR2* and *VISR* expression on MARCO$^-$ macrophages; and high ratios of *PDCD1*, *HAVCR2*, *LAG3* and *TIGIT* expression on activated CD8$^+$ T cells or Tregs (all P < 0.05, Supplementary figure 3d). These results showed that CHI3L1$^+$ stromal cells were part of immunosuppressive TME in UCB tissues.

Our previous studies showed that PD-L1$^+$ immune cells were associated with inferior OS/RFS, aggressive clinical features and high stromal CD8$^+$ tumor-infiltrating lymphocytes (TILs) and PD-1$^+$ TILs in UCB patients.[23] In the current study, we observed that CHI3L1$^+$ stromal cells were co-localised with PD-L1$^+$ immune cells, PD-1$^+$ TILs and CD8$^+$ TILs in neighbouring regions within UCB tissues (Figure 4d). MIF staining also illustrated the wide co-distribution of CHI3L1 with PD-L1, PD-1 and CD8 in the same region of UCB tissues (Supplementary figure 4). The proportion of patients exhibiting both CHI3L1$^+$ stromal cells and PD-L1$^+$ immune cells in tumor tissues was significantly higher in LN$^+$ patients than in LN$^-$ patients (72.7% vs. 34.9%; P < 0.001; Figure 4e). Moreover, CHI3L1$^+$ stromal cells with high densities of stromal CD8$^+$ TILs or PD1$^+$ TILs were associated with tumor lymphatic metastasis (P = 0.023 and 0.029, respectively, Figure 4f and g). We further evaluated the combined impact of CHI3L1$^+$ stromal cells and PD-L1$^+$ immune cells on patient survival (all P < 0.05, Figure 4h and i). We classified the patients into negative or positive groups, based on binary scoring, according to PD-L1 expression in immune cells (≥ 5% of the tumor) and found PD-L1$^+$ immune cells in 57.3% of the UCB patients (98/171). Based on negative/positive CHI3L1$^+$ stromal cells or PD-L1$^+$ immune cells, patients were categorised into three different immune subtypes: (a) both negative (n = 54); (b) either positive (n = 48) and (c) both positive (n = 69). The highest mortality and recurrence rates were observed between groups *a* and *c* (all P < 0.001, Figure 4h and i). These findings established a robust connection between CHI3L1$^+$ stromal cells with PD-L1$^+$ immune cells and diminished survival in UCB patients.

Based on median PD-1$^+$ TIL density (11 cells/field; n = 47) and CD8$^+$ TIL density (55 cells/field; n = 83), PD-1$^+$ TILs were present in 57.4% (27/47) and CD8$^+$ TILs in 48.2% (40/83) of the UCB patients. According to negative/positive CHI3L1$^+$ stromal cells or PD-1$^+$ TIL/CD8$^+$ TIL densities, patients were categorised into three different immune subtypes: (*a*) CHI3L1$^-$ stromal cells with low PD-1$^+$ TILs (n = 16) or CD8$^+$ TILs (n = 26); (*b*) CHI3L1$^+$ stromal cells with low PD-1$^+$

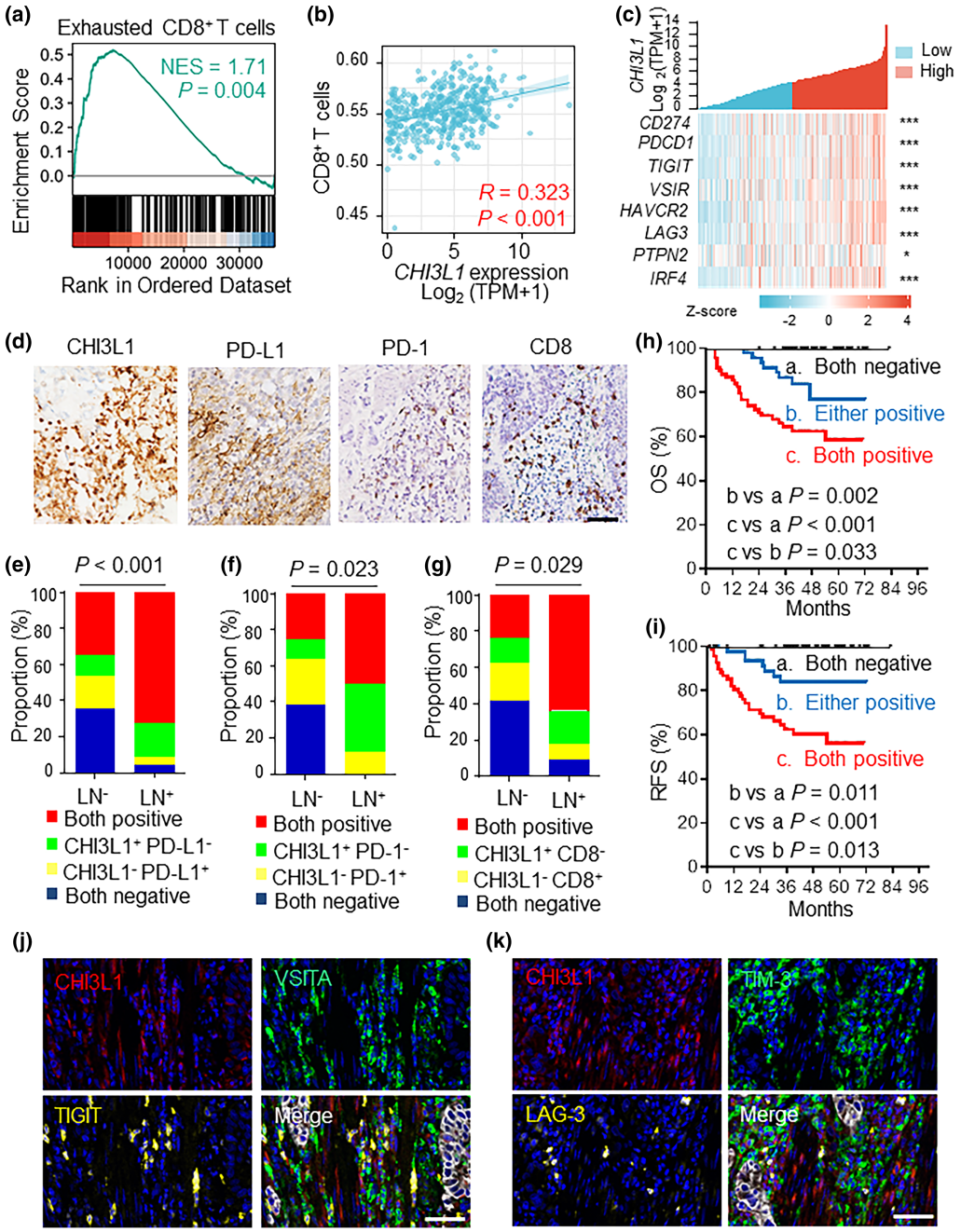

Figure 4. CHI3L1$^+$ stromal cells in immunosuppressive bladder tumor microenvironment. **(a)** Gene set enrichment analysis results reveal the enrichment of the 'Exhausted CD8$^+$ T-cells' pathway in urothelial carcinoma of the bladder (UCB) patients with high *CHI3L1* expression in the TCGA-BLCA cohort. **(b)** Scatter plots illustrate the association between *CHI3L1* expression and the presence of CD8$^+$ T cells. **(c)** Heatmap displaying immune-suppressive genes and their expression to *CHI3L1* in the TCGA-BLCA cohort. **(d)** Representative images depicting the presence of CHI3L1$^+$ stromal cells (SCs), PD-L1$^+$ immune cells (ICs), PD-1$^+$ TIL and CD8$^+$ TIL infiltration in UCB tissues. Scale bars, 50 μm. **(e–g)** Associations of combined CHI3L1$^+$ SCs with PD-L1$^+$ ICs, PD-1$^+$ TILs or CD8$^+$ TILs with lymph node (LN) metastasis in UCB tissues. **(h, i)** Prognostic value of combined CHI3L1$^+$ SCs with PD-L1$^+$ ICs for overall survial (OS) **(h)** and recurrence-free survival (RFS) **(i)** in UCB tissues. **(j)** Representative images of four-colour MIF staining displaying CHI3L1 (red), VSITA (green), TIGIT (yellow) and CK (white), with counterstaining using DAPI (blue). Scale bars, 50 μm. **(k)** Representative images of four-colour immunofluorescence staining revealing CHI3L1 (red), TIM-3 (green), LAG-3 (yellow) and CK (white), with counterstaining using DAPI (blue). Scale bars represent 50 μm. Statistical significance was determined by the unpaired *t*-test and is indicated by *P*-values. **P* < 0.05; ****P* < 0.001.

TILs and CHI3L1$^-$ stromal cells with high PD-1$^+$ TILs (n = 18) or CHI3L1$^+$ stromal cells with low CD8$^+$ TILs and CHI3L1$^-$ stromal cells with high CD8$^+$ TILs (n = 26); and (*c*) CHI3L1$^+$ stromal cells with high PD-1$^+$ TILs (n = 13) or CD8$^+$ TILs (n = 31). The OS and RFS were significantly different between immune subtypes, whereas subtypes of CHI3L1$^-$ stromal cells with low PD-1$^+$ TILs/CD8$^+$ TILs were associated with the most favorable prognosis, respectively ($P < 0.0001$, Supplementary figure 5).

MIF staining further illustrated the wide co-distribution of CHI3L1$^+$ stromal cells with other immunosuppressive molecules, such as TIGIT, VSITA, TIM-3 and LAG-3 (Figure 4j and k), suggesting the potential role of CHI3L1$^+$ stromal cells in orchestrating immune evasion to facilitate bladder cancer metastasis.

DISCUSSION

The impact of inflammation-associated lymphangiogenesis on tumor progression remains a subject of debate.[24] Our results found that proinflammatory cytokine CHI3L1 that were predominately expressed by stromal cells were positively associated with LN metastasis and predicted poor OS and RFS in UCB patients. CHI3L1$^+$ stromal cells were prominently located within densely populated lymphatic vessel niches within immunosuppressive TME. Furthermore, the co-occurrence of CHI3L1$^+$ stromal cells and PD-L1$^+$ immune cells was associated with diminished survival outcomes in UCB patients. These findings suggested that stromal CHI3L1 collaborated with lymphangiogenic and immunosuppressive molecules to influence LN metastasis and tumor progression.

CHI3L1 exhibits widespread expression in numerous human cancers, often correlating with unfavorable prognostic outcomes.[25–27] Previous studies have demonstrated that CHI3L1 is expressed by tumor cells in 22.6% to 50.7% of patients with various tumor types, including papillary thyroid carcinoma, colorectal cancer, breast cancer and glioma.[25,28–30] However, these studies have predominantly focused on the impact of CHI3L1 expression in tumor cells on cancer prognosis, with limited sample sizes and no exploration of the correlation between CHI3L1 expression and lymphatic metastasis. Our study revealed that CHI3L1 expression in stromal cells was approximately 7.5 times higher than its expression in tumor cells in UCB patients. Furthermore, CHI3L1$^+$ stromal cells, as opposed to CHI3L1$^+$ tumor cells, have been established as independent predictors of reduced OS in multivariate Cox analysis and are positively associated with aggressive clinical features. Consistent with our findings, a previous study indicated that CHI3L1$^+$ stromal cells were an independent prognostic factor to a poor prognosis in colorectal cancer.[31] A re-analysis of data from a public scRNA-seq database described the expression of *CHI3L1* by fibroblasts, macrophages and Tregs in human bladder cancer tissues. Surprisingly, muscle cells were found to be one of the potential sources of CHI3L1 in bladder cancer tissues, suggesting that the intrinsic muscle layer components in bladder tissue may also be involved in regulating TME. Although our results showed that tumor cells were not the main producer of CHI3L1 in bladder tumor tissues, Taifour *et al*.[32] showed that secretion of the cytokine CHI3L1 by breast tumor cells induces T-cell exclusion via neutrophil extracellular trap formation in mouse models. Therefore, further research is needed to explore the mechanisms of CHI3L1 from various sources in the progression and metastasis of bladder cancer.

Our previous studies have shown that VEGF-C-promoting lymphangiogenesis is positively associated with regional LN metastasis in bladder cancer.[33] Moreover, blockade of the VEGF-C/VEGFR-3 lymphangiogenic pathway substantially reduced the rate of LN metastasis in mouse models of bladder cancer.[33] In our RNA-sequencing cohort, we observed a significant positive association between *CHI3L1* and *VEGFC*, as well as another lymphangiogenic growth factor, *PDGFB*. Additionally, CHI3L1$^+$ stromal cells and LVD exhibited a positive association within UCB tissues. These findings suggested that CHI3L1 may contribute to lymph metastasis by modulating the lymphangiogenesis pathway in UCB patients. A substantial body of evidence has shown that CHI3L1 plays a crucial role in angiogenesis during tumor progression.[14,15,27] CHI3L1 can stimulate angiogenesis by interacting with proteoglycan and syndecan-1, promoting the release of VEGFA in melanoma cancer.[34] However, our results indicated no significant association between CHI3L1$^+$ stromal cells and MVD within UCB tissues, and *CHI3L1* expression was negatively correlated with *VEGFA* expression. Hence, the impact of CHI3L1 on tumor angiogenesis or lymphangiogenesis might vary based on the specific TME, and additional research is necessary to uncover the underlying mechanisms.

Many studies have found substantial evidence of a strong connection between an immunosuppressive TME and the occurrence of tumor LN metastasis.[35–37] The expression of PD-L1 by either tumor cells or stromal cells has the potential to induce T-cell dysfunction, thereby fostering tumor cell survival and facilitating metastasis.[35–37] In our previous work, we observed a significant correlation between high PD-L1 expression and LN metastasis, as well as an adverse prognosis in UCB.[23] In this study, we further detected positive associations between CHI3L1$^+$ stromal cells and PD-L1$^+$ immune cells, PD-1$^+$ TILs and CD8$^+$ TILs within the stromal regions of UCB tissues. It was evident that patients with both CHI3L1$^+$ stromal cells and PD-L1$^+$ immune cells experienced substantially lower OS and RFS. Furthermore, MIF staining showed that CHI3L1 was co-located with other immunosuppressive molecules, including TIGIT, VSITA, TIM-3 and LAG-3. Recent investigations have revealed that CHI3L1 can regulate the expressions of PD-L1, PD-L2, PD-1, LAG3 and TIM3, by playing a pivotal role in the progression of melanoma and lymphatic metastasis.[16,38] Moreover, simultaneous targeting of CHI3L1 and the PD-1/PD-L1 axis synergistically enhances antitumor responses *in vivo* melanoma models.[16] However, further exploration is required to understand the intricate mechanisms through which CHI3L1 regulates TME and lymphangiogenesis.

This study has a few limitations. First, the retrospective design of this study may have introduced biases and confounding factors. Relevant prospective studies are warranted to verify the results in the future. Second, CHI3L1$^+$ stromal cells compose diverse immune cells, fibroblast cells and even muscle cells. Further studies are needed to determine the cellular source of stromal CHI3L1 in different TMEs and explore the influence of distinct stromal cell types in the functions and mechanisms associated with CHI3L1 expression in the lymphatic metastasis of bladder cancer.

In summary, our findings indicated that CHI3L1 was primarily expressed by stromal cells, with limited expression by tumor cells in UCB tissues. Only elevated levels of CHI3L1 in stromal cells were predictive of an unfavorable prognosis and demonstrated a positive association with lymphatic metastasis. We observed a significant positive correlation between CHI3L1 expression and lymphangiogenic markers as well as immunosuppressive molecules in the stromal regions. These results shed new light on the roles of CHI3L1 in lymphatic metastasis and solidify its status as an indicator of poor prognosis in bladder cancer.

METHODS

Study approval

The study was approved by the SYMH ethical committee and written informed consent was acquired from all patients. The study was conducted per the Declaration of Helsinki.

Patient and tissue samples

The patient enrolment process is shown in Supplementary figure 6. Initially, patients who had undergone transurethral resection of bladder tumors or radical cystectomy for UCB at SYMH were enrolled in two UCB cohorts. UCB cohort I composed of 50 UCB tumoral tissues and 8 peri-tumoral tissues for RNA-seq, which were collected between March 2018 and April 2019, to identify key molecules associated with lymphatic metastasis. Details of clinicopathological characteristics of UCB cohort I were provided in Supplementary table 1. UCB cohort II was composed of 244 UCB patients, whose tissues were collected between June 2006 and May 2017, and were utilised for IHC and MIF analysis. The clinicopathological characteristics of the UCB cohort II were outlined in Supplementary table 2. Additionally, RNA-seq and clinical data for the TCGA-BLCA cohort (n = 408) were obtained from https://portal.gdc.cancer.gov/. Detailed clinicopathological characteristics for the TCGA-BLCA cohort are provided in Supplementary table 3.

Tumors were graded according to the World Health Organization 2016 classification and staged as per the TNM classification (AJCC, 8th edition, 2017).[1] Postoperative follow-up assessments were conducted at intervals of 3 months in the first year, followed by semi-annual checks during the second year and, subsequently, on an annual basis. The median follow-up of the surviving patients was 46 months (range, 16 to 83 months). Of the 244 patients in UCB cohort II, 53 (21.7%) died and 191 (78.3%) survived during the follow-up. OS was characterised as the duration spanning from the date of surgery to either the date of death or the most recent observation. RFS was defined as the time between the surgical procedure and either the occurrence of recurrence or the most recent observation.

RNA-seq

RNA-seq was performed on fresh UCB samples from 50 patients in UCB cohort I at the HaploX Genomics Center (Shenzhen, China). Approximately 30 mg of UCB samples were ground using TRIzol reagent (#12183555, Thermo Fisher Scientific, MA, USA) for total RNA extraction. RNA purity was measured using NanoDrop (#840-343700, Thermo Fisher Scientific, MA, USA), and RNA concentration was verified with Qubit RNA BR Assay Kit (#Q10210t, Thermo Fisher Scientific, CA, USA). Depending on the total amount of RNA, 0.1–1 μg of total RNA was applied to mRNA isolation using the NEBNext Poly(A) mRNA Magnetic

Isolation Module Kit (#E7490L, New England Biolabs, MA, USA). Subsequently, mRNA libraries were constructed with the NEBNext Ultra II mRNA Library Prep Kit for Illumina (#E7760L, New England Biolabs, MA, USA). The concentration of the library was measured with the Qubit dsDNA HS Assay Kit (#Q32854, Thermo Fisher Scientific, CA, USA), and then the fragment distribution of the library was analysed with a D1000 screening tape (#5067-5584, Agilent Technologies, CA, USA). Lastly, library molar concentrations were measured with KAPA Library Quant Kit (Illumina) Universal qPCR Mix (#KK4824-07960140001, Kapa Biosystems, MA, USA). Sequencing of libraries was conducted with the NovaSeq 6000 instrument (Illumina) and the companion NovaSeq S4 kit (#20012866, Illumina Inc, CA, USA). Raw sequencing data in FASTQ format were available from the NovaSeq 6000 instrument, and quality control read comparison and transcript quantification were performed.

IHC and MIF analyses

Formalin-fixed and paraffin-embedded samples from UCB cohort II were cut into 5 μm sections and processed for IHC and MIF staining as previously described.[23,39] For IHC, briefly, after dewaxing, rehydrating, antigen retrieval, inactivating endogenous peroxidase and blocking non-specific binding, 5-μm-thick sections were incubated with anti-CHI3L1 (1:800, #47066S, Cell Signaling Technology, MA, USA) overnight at 4°C. Subsequently, sections were incubated with the corresponding secondary antibody (Vector Peterborough, UK) and stained with peroxidase and 3,3′-diaminobenzidine tetrahydrochloride in EnVision Detection System (#K5007, Dako, CO, USA). Finally, slides were counterstained with haematoxylin. The sections were captured within ×400 high-power fields by an ECLIPSE Ni-E/Ni-U microscope (Nikon, Tokyo, Japan) and analysed by manual counting.

MIF staining was performed using a PANO 4-plex MIF Kit (#0079100020, Panovue, Beijing, China) following the manufacturer's protocol.[39] Briefly, sections were deparaffinised and hydrated. A microwave treatment was applied for antigen retrieval. After a 10-min blocking step, sections were incubated with the primary antibodies at 4°C overnight. Next, the slices were incubated with the corresponding secondary antibodies (Vector Peterborough, UK) at 37°C for 10 min. Finally, one of the four tyramide signal amplification fluorophores (Opal 520, 570, 620 and 690) was added to the tissue sections for 10 min. This sequence of steps (except deparaffinisation and hydration) was repeated, starting with blocking and ending with the microwave treatment. The slides were scanned with a Vectra Polaris Automated Quantitative Pathology Imaging System (PerkinElmer, Waltham, USA). The signals were evaluated and quantified using Phenochart and inForm Tissue Analysis software (PerkinElmer). The primary antibodies used for the MIF staining were as follows: anti-CHI3L1 (1:1000, #47066S, Cell Signaling Technology, MA, USA); anti-CD105 (1:3000, #14606S, Cell Signaling Technology, MA, USA); anti-D2-40 (1:1000, #ZM-0465, ZSGB-Bio, Beijing, China); anti-cytokeratin (CK, #TA309725, ZSGB-Bio), anti-LAG-3 (1:2000, #15372S, Cell Signaling Technology, MA, USA); anti-TIM-3 (1:2000, #81229S, Cell Signaling Technology, MA, USA); anti-VISTA (1:2000, #64953S, Cell Signaling Technology, MA, USA) and anti-TIGIT (1:1000, #99567S, Cell Signaling Technology, MA, USA).

Evaluation of IHC and MIF staining

Tissue sections were analysed by two independent observers who were blinded to the clinical outcome. The staining data of PD-L1, PD-1 and CD8 by IHC were obtained from previous studies.[23,39] CHI3L1-positive expression was defined as a moderate and robust cytoplasmic expression of $> 5\%$ stained cells in IHC staining.[25,31] For PD-L1, $< 5\%$ IHC staining pattern was considered negative and $\geq 5\%$ was considered positive.[23] IHC staining for the density of PD-1$^+$ TILs and CD8$^+$ TILs was assessed at five representative high-power fields in IHC staining (400× magnification, 0.07 mm^2/field) and counted manually.

MVD was calculated as the number of micro-vessels per tumor area, while LVD was calculated as the number of lymphatic vessels per tumor area. Slides stained for CD105 and D2-40 were counted to determine MVD and LVD respectively. The MIF staining of CHI3L1, D2-40 and CD105 was evaluated by capturing images in the same field of vision (200× magnification, 0.18 mm^2/field) and counted manually. Twenty-one zones were randomly defined and quantified for five UCB patients to analyse the correlations between CHI3L1$^+$ SCs and D2-40$^+$ LVD/ CD105$^+$ MVD. To analyse the relationship between CHI3L1 and immunosuppressive molecules, the MIF staining of CHI3L1, LAG-3, TIM-3, VISTA and TIGIT were evaluated by capturing images in the same field of vision (200× magnification, 0.18 mm^2/field).

qRT-PCR assay

Total RNA was extracted from UCB tissues using the RNA Quick Purification Kit (#RN001, YISHAN Biotechnology, Shanghai, China). RNA was reverse transcribed into cDNA using a cDNA Synthesis Kit (#R212-02, Vazyme, Nanjing, China). The qRT-PCR was performed using the SYBR Green PCR Kit (#D7268M, Beyotime, Shanghai, China). Gene expression was calculated using the $2^{-\Delta\Delta Ct}$ method. The expression of target genes was normalised to GAPDH and displayed as a fold change relative to the control groups. The primers are listed in Supplementary table 4.

scRNA-seq

The scRNA-seq data for eight primary tumors of bladder cancer (two low-grade bladder urothelial tumors and six high-grade bladder urothelial tumors) were retrieved[22] from the DISCO scRNA repository (https://www.immunesinglecell.org/repository). Quality control and data integration were performed using the built-in fast integration tool provided in platform.[40] Downstream analyses were conducted by using the R language. To obtain a UMAP plot with clustering annotations, we employed the DimPlot function from the Seurat package. The expression distribution of the target gene across cell types was explored by utilising the FeaturePlot function. We further employed the ggplot2 package to visualise the

density distribution of gene expression across the samples. Based on the central tendency of the distribution of *CHI3L1*$^+$ fibroblasts, we divided the samples into high-expression and low-expression groups for the target gene. To visualise the distribution of immune suppressive-related genes across cell types within the two groups, violin plots were used to display the expression patterns. Non-parametric rank-sum tests were employed to assess the statistical significance of differences in gene expression distribution across cell types between the two expression groups of *CHI3L1*. $P < 0.05$ was considered statistically significant.

Bioinformatic analysis

The DESeq2 package was applied to identify DEGs of LRGs (LN^+ vs. LN^-) and TRGs (tumor vs. peri-tumor) in UCB cohort I. The criteria for DEGs consisted of gene expression alteration with $|\log2 \text{ fold change}| \geq 1$. The Venn package was used to identify the intersection genes between LRGs and TRGs, selecting the lymphatic metastasis-related key genes. In the TCGA-BLCA cohort, the DEGs were performed to identify the *CHI3L1*-related genes. GSEA was conducted for the enrichment of gene expression in biological functions and pathways of DEGs of *CHI3L1*-related genes, with the criterion of $P < 0.05$ and false discovery rate (FDR) < 0.25. The cluster profile and ggplot2 package were employed for visualisation. In addition, the association of *CHI3L1* and LRGs and immunosuppression-related genes in the TCGA-BLCA cohort was analysed using Spearman's correlation analysis. The R package, pheatmap, was used to draw the heat maps. The association of *CHI3L1* with immune cells was assessed using single-sample GSEA. The single-sample GSEA can determine the immune cell population in a tumor sample according to gene expression data.[41] The GSVA package of R and immune datasets was used to determine the infiltration level of immune cells in the TCGA-BLCA cohort.

Nomogram for predicting 3- and 5-year survival

The coefficients calculated by the multivariate Cox model were used to generate the nomogram. A nomogram was created combining CHI3L1$^+$ stromal cells and TNM stage to predict the 3- and 5-year OS. To verify the accuracy of the nomogram model, a calibration curve was developed. A decision curve analysis was also performed for predicting 3- and 5-year OS in the nomogram model. To further compare the sensitivity and specificity of the current nomogram model with the TNM stage, a receiver–operator characteristic analysis was performed and the AUC was concurrently calculated.

Statistical analysis

Statistical analyses were conducted using SPSS 18.0 Statistical Software (IBM). Data are presented as means ± standard error of the mean (SEM) and $P < 0.05$ was considered significant. Continuous variables were compared using the Mann–Whitney *U*-test, while the comparison of categorical variables was conducted using Pearson's chi-square test or Fisher's exact test as appropriate. Cumulative survival time was calculated to explore the prognostic significance of CHI3L1 in UCB by using the Kaplan–Meier method and compared using the log-rank test. To evaluate the independent risk factors for the prognosis of UCB, univariate and multivariate Cox analyses were performed. The multivariate Cox analysis was performed by the multivariate Cox proportional hazard model, including all significant covariates ($P < 0.1$) from the univariate Cox model. Relative risks are expressed as odds ratios with a 95% confidence interval.

ACKNOWLEDGMENTS

This study was supported by the National Key Research and Development Program of China (Grant No. 2018YFA0902803); the National Natural Science Foundation of China (Grant No. 82000198, 81825016, 81961128027, 81772719, 81772728 and 81902582); The Key Areas Research and Development Program of Guangdong (Grant No. 2018B010109006); the Science and Technology Planning Project of Guangdong Province (Grant No. 2017B020227007; 2022A151501110); the Guangdong Provincial Clinical Research Center for Urological Diseases (2020B1111170006); the Medical Scientific Research of Guangdong Province (Grant No. A2019470) and the Administration of Traditional Chinese Medicine of Guangdong Province (Grant No. 20201119).

AUTHOR CONTRIBUTIONS

Bo Wang: Data curation; methodology; writing – original draft. **Ke Chen:** Data curation; formal analysis; methodology; writing – original draft. **Mingchao Gao:** Data curation; formal analysis; methodology; writing – original draft. **Xi Sun:** Data curation; investigation. **Wang He:** Writing – review and editing. **Junyu Chen:** Methodology. **Wenjuan Yang:** Data curation; investigation. **Tenghao Yang:** Data curation; investigation. **Haide Qin:** Formal analysis; software; visualization. **Honglian Ruan:** Formal analysis; software; visualization. **Hao Huang:** Supervision; writing – review and editing. **Tianxin Lin:** Supervision; writing – review and editing. **Jian Huang:** Conceptualization; funding acquisition; project administration.

CONFLICT OF INTEREST

The authors declare no conflict of interest.

DATA AVAILABILITY STATEMENT

The data that support the results of this study can be supplied upon request.

ETHICS APPROVAL

All participants gave their informed consent to use data for this retrospective study involving human participants. The institutional ethical committees of the hospital approved the study. The study was performed in accordance with the Declaration of Helsinki.

REFERENCES

1. Kamoun A, de Reyniès A, Allory Y *et al*. A consensus molecular classification of muscle-invasive bladder cancer. *Eur Urol* 2020; **77**: 420–433.
2. Liu S, Chen X, Lin T. Lymphatic metastasis of bladder cancer: molecular mechanisms, diagnosis and targeted therapy. *Cancer Lett* 2021; **505**: 13–23.
3. Karl A, Carroll PR, Gschwend JE *et al*. The impact of lymphadenectomy and lymph node metastasis on the outcomes of radical cystectomy for bladder cancer. *Eur Urol* 2009; **55**: 826–835.
4. Deng H, Zhang J, Wu F *et al*. Current status of lymphangiogenesis: molecular mechanism, immune tolerance, and application Prospect. *Cancer* 2023; **15**: 1169.
5. Ladányi A, Tímár J. Immunologic and immunogenomic aspects of tumor progression. *Semin Cancer Biol* 2020; **60**: 249–261.
6. Wang CA, Tsai SJ. The non-canonical role of vascular endothelial growth factor-C axis in cancer progression. *Exp Biol Med (Maywood)* 2015; **240**: 718–724.
7. Karaman S, Detmar M. Mechanisms of lymphatic metastasis. *J Clin Invest* 2014; **124**: 922–928.
8. Kzhyshkowska J, Gratchev A, Goerdt S. Human chitinases and chitinase-like proteins as indicators for inflammation and cancer. *Biomark Insights* 2007; **2**: 128–146.
9. Huang J, Gu Z, Xu Y, Jiang L, Zhu W, Wang W. CHI3L1 (chitinase 3 like 1) upregulation is associated with macrophage signatures in esophageal cancer. *Bioengineered* 2021; **12**: 7882–7892.
10. Zhao T, Su Z, Li Y, Zhang X, You Q. Chitinase-3 like-protein-1 function and its role in diseases. *Signal Transduct Target Ther* 2020; **5**: 201.
11. Johansen JS, Jensen BV, Roslind A, Nielsen D, Price PA. Serum YKL-40, a new prognostic biomarker in cancer patients? *Cancer Epidemiol Biomarkers Prev* 2006; **15**: 194–202.
12. Yeo IJ, Lee CK, Han SB, Yun J, Hong JT. Roles of chitinase 3-like 1 in the development of cancer, neurodegenerative diseases, and inflammatory diseases. *Pharmacol Ther* 2019; **203**: 107394.
13. Hao H, Chen H, Xie L, Liu H. YKL-40 promotes invasion and metastasis of bladder cancer by regulating epithelial mesenchymal transition. *Ann Med* 2021; **53**: 1170–1178.
14. Shao R, Hamel K, Petersen L *et al*. YKL-40, a secreted glycoprotein, promotes tumor angiogenesis. *Oncogene* 2009; **28**: 4456–4468.
15. Shao R. YKL-40 acts as an angiogenic factor to promote tumor angiogenesis. *Front Physiol* 2013; **4**: 122.
16. Ma B, Akosman B, Kamle S *et al*. CHI3L1 regulates PD-L1 and anti-CHI3L1-PD-1 antibody elicits synergistic antitumor responses. *J Clin Invest* 2021; **131**: e137750.
17. Cintin C, Johansen JS, Christensen IJ, Price PA, Sørensen S, Nielsen HJ. Serum YKL-40 and colorectal cancer. *Br J Cancer* 1999; **79**: 1494–1499.
18. Johansen JS, Christensen IJ, Jørgensen LN *et al*. Serum YKL-40 in risk assessment for colorectal cancer: a prospective study of 4,496 subjects at risk of colorectal cancer. *Cancer Epidemiol Biomarkers Prev* 2015; **24**: 621–626.
19. Tarpgaard LS, Guren TK, Glimelius B *et al*. Plasma YKL-40 in patients with metastatic colorectal cancer treated with first line oxaliplatin-based regimen with or without cetuximab: RESULTS from the NORDIC VII study. *PLoS One* 2014; **9**: e87746.
20. Pereira ER, Kedrin D, Seano G *et al*. Lymph node metastases can invade local blood vessels, exit the node, and colonize distant organs in mice. *Science* 2018; **359**: 1403–1407.
21. Lucas ED, Finlon JM, Burchill MA *et al*. Type 1 IFN and PD-L1 coordinate lymphatic endothelial cell expansion and contraction during an inflammatory immune response. *J Immunol* 2018; **201**: 1735–1747.
22. Chen Z, Zhou L, Liu L *et al*. Single-cell RNA sequencing highlights the role of inflammatory cancer-associated fibroblasts in bladder urothelial carcinoma. *Nat Commun* 2020; **11**: 5077.
23. Wang B, Pan W, Yang M *et al*. Programmed death ligand-1 is associated with tumor infiltrating lymphocytes and poorer survival in urothelial cell carcinoma of the bladder. *Cancer Sci* 2019; **110**: 489–498.
24. Alitalo K, Tammela T, Petrova TV. Lymphangiogenesis in development and human disease. *Nature* 2005; **438**: 946–953.
25. Zhang JP, Yuan HX, Kong WT *et al*. Increased expression of chitinase 3-like 1 and microvessel density predicts metastasis and poor prognosis in clear cell renal cell carcinoma. *Tumour Biol* 2014; **35**: 12131–12137.
26. Luo D, Chen H, Lu P *et al*. CHI3L1 overexpression is associated with metastasis and is an indicator of poor prognosis in papillary thyroid carcinoma. *Cancer Biomark* 2017; **18**: 273–284.
27. De Robertis M, Greco MR, Cardone RA *et al*. Upregulation of YKL-40 promotes metastatic phenotype and correlates with poor prognosis and therapy response in patients with colorectal cancer. *Cells* 2022; **11**: 3568.
28. Kim SH, Das K, Noreen S, Coffman F, Hameed M. Prognostic implications of immunohistochemically detected YKL-40 expression in breast cancer. *World J Surg Oncol* 2007; **5**: 17.
29. Steponaitis G, Skiriutė D, Kazlauskas A *et al*. High CHI3L1 expression is associated with glioma patient survival. *Diagn Pathol* 2016; **11**: 42.
30. Shao R, Cao QJ, Arenas RB, Bigelow C, Bentley B, Yan W. Breast cancer expression of YKL-40 correlates with tumour grade, poor differentiation, and other cancer markers. *Br J Cancer* 2011; **105**: 1203–1209.
31. Oh IH, Pyo JS, Son BK. Prognostic impact of YKL-40 immunohistochemical expression in patients with colorectal cancer. *Curr Oncol* 2021; **28**: 3139–3149.
32. Taifour T, Attalla SS, Zuo D *et al*. The tumor-derived cytokine Chi3l1 induces neutrophil extracellular traps that promote T cell exclusion in triple-negative breast cancer. *Immunity* 2023; **56**: 2755–2772.e2758.
33. He W, Zhong G, Jiang N *et al*. Long noncoding RNA BLACAT2 promotes bladder cancer-associated lymphangiogenesis and lymphatic metastasis. *J Clin Invest* 2018; **128**: 861–875.
34. Ramos-Espinosa G, Wang Y, Brandner JM, Schneider SW, Gorzelanny C. Melanoma associated chitinase 3-like 1 promoted endothelial cell activation and immune cell recruitment. *Int J Mol Sci* 2021; **22**: 3912.

35. Chen L, Han X. Anti-PD-1/PD-L1 therapy of human cancer: past, present, and future. *J Clin Invest* 2015; **125**: 3384–3391.
36. Teng MW, Ngiow SF, Ribas A, Smyth MJ. Classifying cancers based on T-cell infiltration and PD-L1. *Cancer Res* 2015; **75**: 2139–2145.
37. Massi D, Brusa D, Merelli B *et al*. PD-L1 marks a subset of melanomas with a shorter overall survival and distinct genetic and morphological characteristics. *Ann Oncol* 2014; **25**: 2433–2442.
38. Ma B, Kamle S, Akosman B *et al*. CHI3L1 enhances melanoma lung metastasis via regulation of T cell co-stimulators and CTLA-4/B7 axis. *Front Immunol* 2022; **13**: 1056397.
39. Hou W, Xue M, Shi J *et al*. PD-1 topographically defines distinct T cell subpopulations in urothelial cell carcinoma of the bladder and predicts patient survival. *Urol Oncol* 2020; **38**: e681–685.e610.
40. Li M, Zhang X, Ang KS *et al*. DISCO: A database of deeply integrated human single-cell omics data. *Nucleic Acids Res* 2022; **50**: D596–D602.
41. Bindea G, Mlecnik B, Tosolini M *et al*. Spatiotemporal dynamics of intratumoral immune cells reveal the immune landscape in human cancer. *Immunity* 2013; **39**: 782–795.

Supporting Information

Additional supporting information may be found online in the Supporting Information section at the end of the article.